



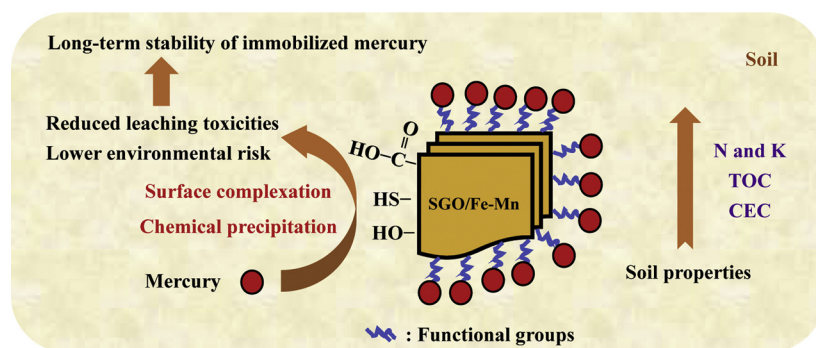
In situ remediation of mercury-contaminated soil using thiol-functionalized graphene oxide/Fe-Mn composite

Yao Huang, Mengxia Wang, Zhanjun Li, Yanyan Gong*, Eddy Y. Zeng

Guangdong Key Laboratory of Environmental Pollution and Health, School of Environment, Jinan University, Guangzhou, 511443, China



GRAPHICAL ABSTRACT



ARTICLE INFO

Keywords:

Mercury
Heavy metals
Thiol-functionalized graphene oxide
Fe-Mn oxides
Soil remediation

ABSTRACT

Mercury (Hg) contamination in soil is a paramount concern to the environment and public health. Yet, effective *in situ* remediation technologies have been lacking. In this study, a novel thiol-functionalized graphene oxide/Fe-Mn (SGO/Fe-Mn) composite was prepared and investigated for *in situ* immobilization of Hg in contaminated soil. Batch tests showed that application of SGO/Fe-Mn at doses of 0.4% and 0.8% effectively reduced H₂O, H₂SO₄ and HNO₃, CH₃COOH, and CaCl₂-extractable Hg by 90.3–98.9% and 96.5–98.9%, respectively, upon equilibrium after 72 d. An increasing of soil moisture content from 0 to 12.5% significantly enhanced the immobilization efficiency from 75.0% to 97.6%. XRD, FTIR, and XPS analyses suggested that the composite mainly immobilized Hg through surface complexation and chemical precipitation. Sequential extraction procedure demonstrated that the composite promoted the conversion of more accessible Hg (exchangeable and carbonate fractions) into the less accessible forms, i.e., oxides, organic matter, and residual fractions, resulting in substantially reduced environmental risk of Hg. The application of SGO/Fe-Mn enhanced soil cation exchange capacity, available N and K, and total organic carbon, and can be used to effectively improve soil properties. Moreover, immobilized Hg in soil by this composite remained stable over one year. The present study demonstrates the potential and viability of SGO/Fe-Mn for enhanced immobilization of Hg in soil and sediment.

1. Introduction

Mercury (Hg) is one of the most pervasive and toxic heavy metals in

the environment. It is generated from a variety of industrial sources such as coal combustion, mining activities, chlor-alkali production, and manufacture of compact fluorescent lamps, cosmetic, insecticides, and

* Corresponding author.

E-mail address: yanyangong@jnu.edu.cn (Y. Gong).

<https://doi.org/10.1016/j.jhazmat.2019.03.132>

Received 16 February 2019; Received in revised form 29 March 2019; Accepted 30 March 2019

Available online 01 April 2019

0304-3894/ © 2019 Elsevier B.V. All rights reserved.

herbicides [1], leading to soil contamination by Hg in surrounding areas. Soil Hg can be readily taken up by agricultural crops [1], and accumulated along the food chain, posing potential threats to human health. Exposure to Hg has been reported to cause various neurodegenerative diseases (i.e., Amyotrophic lateral sclerosis, Alzheimer's diseases, and Parkinson's disease) [1,2], to damage the immune system and kidneys [3], and to harm the cardiovascular and nervous systems [4]. Apparently, Hg-contaminated soil requires substantial remediation if the extent of contamination poses unacceptable risk to human health or the environment.

Several remediation technologies have been developed for treating Hg-contaminated soil, such as soil washing [5], thermal desorption [6–8], electrokinetic remediation [9], and phytoextraction [10], which aim to remove Hg from soil to achieve target cleanup thresholds. However, these technologies are pegged with significant drawbacks. For instance, the chemical agents applied in soil washing may cause potential adverse effects, and wastewater thus produced must be further handled or treated. Reducing total concentrations of soil Hg can also be quite costly. The recent trend has been shifting to reduction of the physicochemical and/or bioavailable fractions of soil heavy metals.

In situ immobilization applies chemical agents to contaminated soil to reduce the mobility, bioavailability, and potential toxicity of soil Hg [1]. Thiol-functionalized sorbents are expected to exhibit fast sorption kinetics, high sorption capacity, and strong binding affinity for Hg as a consequence of soft Lewis acid-base interaction [4]. He et al. [11] found that sorption of Hg^{2+} to thiol-functionalized Zn-doped biomagnetite particles equilibrated at 30 min, compared to 3–8 h for other commercial sorbents, at pH 8.0 in industrial wastewater. Niu et al. [12] demonstrated that thiol-functionalized polysilsesquioxanes had high selectivity for Hg^{2+} from aqueous solutions in the presence of Mn^{2+} , Cu^{2+} , Pb^{2+} , Co^{2+} , and Ni^{2+} , all at an initial concentration of $0.002 \text{ mmol L}^{-1}$. Zhang et al. [13] applied thiol-modified zeolite (TFZ) to immobilize Hg in solid wastes and observed significantly lowered toxicity characteristic leaching procedure (TCLP) leachable mercury concentrations. As the TFZ dosage increased from 0% to 5.0%, the TCLP-leachable mercury concentration was reduced from more than 2 mg L^{-1} to less than 0.1 mg L^{-1} . O'Connor et al. [14] successfully modified rice husk biochar with non-toxic elemental sulfur (S) and revealed that the S modification increased the mercury uptake by 73%. When S-modified biochar (dosages of 1%, 2%, and 5%, respectively) was applied to treat Hg-contaminated soil (1000 mg kg^{-1}), the TCLP leachable Hg was dramatically decreased by up to 99.3% compared to that of untreated soil. Our previous study developed a novel thiol-functionalized graphene oxide/Fe-Mn (SGO/Fe-Mn) via an ammonium hydroxide method and demonstrated its strong sorption affinity and high sorption capacity for both inorganic and organic Hg from aqueous solutions. The maximum sorption capacity reached 233 mg g^{-1} for Hg^{2+} and 36.7 mg g^{-1} for CH_3Hg^+ , much greater than those of other mercury sorbents [15]. Yet, the immobilization effectiveness and mechanisms of soil Hg by SGO/Fe-Mn as well as the long-term stability of immobilized mercury have not been examined.

The present study was conducted to determine the feasibility of SGO/Fe-Mn for immobilizing Hg in contaminated soil, and its objectives were to (1) test the effects of treatment time, SGO/Fe-Mn dosage, and soil moisture content on Hg immobilization effectiveness; (2) probe any change in soil-bound Hg speciation before and after treatment, evaluate the environmental risk, and explore the underlying immobilization mechanisms; (3) assess the impacts of SGO/Fe-Mn on physicochemical properties of soil; and (4) evaluate the long-term stability (over one year) of immobilized Hg in soil.

2. Materials and methods

2.1. Materials

All chemicals used in this study were of analytical grade or higher.

Graphene oxide (GO) was obtained from Ailian Electronic Technology (Tianjin, China). 3-mercaptopropyltrimethoxysilane (3-MPTS) and ethanol were purchased from J&K Scientific (Beijing, China). $\text{Hg}(\text{NO}_3)_2 \cdot \text{H}_2\text{O}$ was purchased from Aikeda Chemical Technology (Chengdu, China). HNO_3 , H_2SO_4 , CaCl_2 , $\text{FeSO}_4 \cdot 7\text{H}_2\text{O}$, KMnO_4 , and NH_4OH (25% NH_3 in H_2O) were procured from Kutai Chemical Reagent Technology (Guangzhou, China).

2.2. Preparation of g-spiked soil and soil analysis

A Hg-free surface soil (0–30 cm) was collected from campus of Nankai University, Tianjin, China. The latitude/longitude of the site was 117.34/38.99. Before use, the samples were air-dried, sieved through a 10-mesh screen, and washed three times with tap water to remove suspended colloids and water leachable compositions. The washed soil was then air dried and stored in a sealed plastic barrel. To facilitate the subsequent Hg immobilization tests, mercury was loaded to the soil following previously reported procedure by Gong et al. [16]. In brief, 5.0 kg of pretreated soil was mixed with 10 L of 160.0 mg L^{-1} $\text{Hg}(\text{NO}_3)_2$ in a closed polyethylene container for 90 d. After 24 h of gravity settling, the supernatant was discarded and the Hg-laden soil was air-dried for 7 d. The air-dried soil was then digested per US Environmental Protection Agency (EPA) Method 3050B and analyzed for aqueous mercury concentration. The final mercury content in the soil was determined to be 195.0 mg kg^{-1} .

Soil analysis was performed by Guangzhou Chemical Union Quality Technology Company. Soil pH was measured in a 1:1 soil:water mixture following the Agricultural Standard of China (NY/T 1377-2007). The chemical compositions of Hg-laden soil was characterized by X-ray fluorescence (XRF) spectrometry (XRF-1700, Shimadzu, Japan). The available N, P, K, and cation exchange capacity (CEC) of soil were tested following the Environmental Protection Standards of China (NY/T 53-1987, HJ 632-2011, NY/T 87-1988, and NY/T 1121.5-2006, respectively). Soil texture was determined following the laser diffraction method using a laser diffractometer (Mastersizer 2000, Malvern, UK), which measures within a size range of 0.02–2000 μm . The total organic carbon was determined by a TOC analyzer (SSM-5000A, Shimadzu, Japan).

2.3. Preparation and characterization of SGO/Fe-Mn composite

SGO/Fe-Mn was prepared following our previously reported method [4,17]. The details are provided in the supplementary information (SI). SGO/Fe-Mn before and after reaction with Hg-laden soil were characterized. SGO/Fe-Mn before reaction was collected directly. SGO/Fe-Mn after reaction with soil was prepared by mixing 0.8 g SGO/Fe-Mn with 100.0 g soil (i.e., 0.8% dosage) at a moisture content of $25 \pm 2\%$ for 72 d. The mixture was freeze-dried under vacuum at -60°C (FD5-3 freeze-dryer, SIM, California, USA) for 48 h, and then collected for characterization tests. The structure and surface morphology was analyzed by a JSM-6400 scanning electron microscopy (SEM) (JEOL, Tokyo, Japan). Fourier transform infrared (FTIR) analysis was carried out by a FTS-6000 spectrometer (Bio-rad, California, USA). The crystalline compositions was identified by X-ray powder diffraction (XRD) using a D/max-2500 powder diffraction meter (Rigaku, Osaka, Japan) with a $\text{Cu K}\alpha$ radiation. Surface elemental compositions were analyzed by X-ray photoelectron spectroscopy (XPS) using a PHI-5000 Versaprobe II spectrometer (ULVAC-PHI, Chigasaki, Japan).

2.4. Immobilization of mercury in soil by SGO/Fe-Mn

Batch immobilization experiments were carried out in 500-mL polyethylene bottles containing 400.0 g of Hg-laden soil with the addition of various dosage of SGO/Fe-Mn, namely, 0.4% and 0.8% by dry weight. 135 mL of deionized (DI) water was added to the mixture to keep a moisture content of $25 \pm 2\%$. The bottles were then sealed and

stored in the dark at room temperature ($25 \pm 2^\circ\text{C}$). At predetermined time intervals (1, 3, 7, 13, 21, 29, 72, 222, and 365 d), 2.0 g of soil (dry weight) was collected and tested for leaching toxicity as described in Section 2.5. All experiments were conducted in triplicates. Control tests were carried out in the absence of SGO/Fe-Mn under otherwise identical conditions.

To evaluate the effects of soil moisture content on mercury immobilization via SGO/Fe-Mn, various moisture contents (0, 7.0%, 14.0%, 25.0%, 32.0%, 40%, 62.5%, and 80.0%) were obtained by adding different volumes of DI water into the mixture of 1.6 g SGO/Fe-Mn and 400.0 g Hg-laden soil (i.e., 0.4% dosage of SGO/Fe-Mn).

2.5. Leaching tests

Standard batch leaching tests were performed by mixing 2.0 g (dry weight) of the untreated and treated sample with 20 mL H_2O , 20 mL H_2SO_4 and HNO_3 solution, 40 mL CH_3COOH solution, and 20 mL CaCl_2 solution, respectively, in 42 mL polyethylene centrifuge tubes to investigate the role of SGO/Fe-Mn in controlling the mobility of mercury. H_2O is used as a washing solution to simulate the process in which the samples are leached by surface water or groundwater (HJ 557-2010, China). The mixture of concentrated H_2SO_4 and HNO_3 at a mass ratio of 2:1 in DI water ($\text{pH} = 3.20 \pm 0.05$) is used to simulate the process in which the samples are leached by acidic rain (HJ/T 299-2007, China). The CH_3COOH solution following the method HJ/T 300-2007 of China is to simulate the process in which the samples are leached under the influence of landfill leachate. 5.7 mL of glacial acetic acid was added to 500.0 mL of DI water, followed by the addition of 64.3 mL of 1.0 mol L^{-1} NaOH and the dilution to 1.0 L, resulting in a final pH of 4.93 ± 0.05 . CaCl_2 solution (0.01 mol L^{-1}) prepared according to the approach by Cao et al. [18] is to assess the bioavailability of mercury in the soil. In all cases, the tubes were sealed and agitated on an end-over-end rotator at 40 rpm at room temperature ($25 \pm 2^\circ\text{C}$) for 8 h, 18 ± 2 h, 18 ± 2 h, and 24 h, respectively. After centrifuging at 4000 rpm for 10 min, the supernatant was filtered through $0.22 \mu\text{m}$ PTFE filters and analyzed for mercury concentration in the filtrates. The immobilization efficiency was calculated via equation (1) [19]:

$$\text{Immobilization efficiency of mercury}(\%) = \left(1 - \frac{M}{M_0}\right) \times 100\% \quad (1)$$

where M and M_0 are the mercury mass (mg) in the leaching supernatants of the treated and untreated soil, respectively.

2.6. Sequential extraction of soil-sorbed Hg

A modified sequential extraction procedure (SEP) developed by Tessier et al. [20] was employed to quantify the relative availability of Hg based on fractions of various operationally defined Hg species (Table S1). The five fractions have been defined as exchangeable (EX), carbonate-bound (CB), Fe-Mn oxides-bound (OX), organic material-bound (OM), and residual (RS) fractions [20], and the relative availability follows the order of $\text{EX} > \text{CB} > \text{OX} > \text{OM} > \text{RS}$ [19].

2.7. Risk assessment code

Risk assessment code (RAC) is a commonly used method for soil risk evaluation of heavy metals [21,22]. EX and CB fractions have the highest bioavailability and the greatest potential to cause secondary environmental pollution. OX and OM fractions are considered as potentially bioavailable states which undergo leaching at very rigorous conditions (e.g., highly acidic or oxidizing conditions) [21]. RS fraction is the most stable state. Heavy metals can be remained in the crystal structure and are not easily leached [21]. RAC value is defined as the fraction ratio of EX and CB to the sum of EX, CB, OX, OM, and RS based on Tessier's SEP as described in Section 2.6 [21,23]:

$$\text{RAC} = \frac{\text{EX} + \text{CB}}{\text{EX} + \text{CB} + \text{OX} + \text{OM} + \text{RS}} \times 100\% \quad (2)$$

The RAC value indicates the proportion of EX and CB fractions with $< 1.0\%$ of the total metal being safe for the environment, $1.0\text{--}10.0\%$ being low risk, $11.0\text{--}30.0\%$ being medium risk, $31.0\text{--}50.0\%$ being high risk, and $> 50.0\%$ being highly dangerous to ecological environment, i.e. very high risk [24].

2.8. Analytical methods

Mercury concentration in the aqueous solution was determined using an atomic fluorescence spectrometer (AFS-933, Titan Instruments, Beijing, China) following the Environmental Protection Standard of China (HJ694-2014). The detection limit was $0.04 \mu\text{g Hg L}^{-1}$. pH was measured using a PB-10 pH meter (Sartorius, Gottingen, Germany).

3. Results and discussion

3.1. Characterization of SGO/Fe-Mn

Pristine GO shows a typical wrinkled and sheet-like structure (Figs. 1A and B). Fe-Mn oxide appeared as aggregated flocs (Fig. 1C). SGO/Fe-Mn exhibits a sheet-like multilayer structure with a large number of wrinkles on the surface (Figs. 1D, E, and F). Fe-Mn oxides are clearly distributed on the surface, interlayer, and edge of GO (Figs. 1E and F) via the interactions between Fe-Mn oxides and functional groups (e.g., hydroxyl, carboxyl, and epoxy) of GO [4,17], resulting in reduced particle size of Fe-Mn. It is noteworthy that Fe-Mn oxide particles with sizes $< 20 \text{ nm}$ mainly distributed on the SGO/Fe-Mn surface, whereas those at 50 nm largely spread at the edges. This pattern is consistent with the distribution of functional groups of GO, which are mainly situated at the edges [4,17].

3.2. Immobilization of Hg-contaminated soil by SGO/Fe-Mn and governing factors

The effect of SGO/Fe-Mn amendments on mercury mobility and bioavailability was examined by extraction with H_2O , H_2SO_4 and HNO_3 , CH_3COOH , and CaCl_2 , respectively, with leachable Hg concentrations at 150.0 , 160.0 , 108.0 , and $207.0 \mu\text{g L}^{-1}$ in untreated soil, respectively. Under all amendment scenarios, the Hg immobilization efficiency was rapidly enhanced as reaction time increased to 13 d, and then gradually increased afterwards until reaching equilibrium at 72 d (Fig. 2). Therefore, 72 d was used in the following tests to ensure the immobilization equilibrium.

As the immobilization time was extended from 0 to 13 d, increasing the SGO/Fe-Mn dosage from 0.4% to 0.8% enhanced the Hg immobilization efficiency (Fig. 2). For instance, the H_2SO_4 and HNO_3 leachable mercury concentration was reduced by 70.8% with 0.4% SGO/Fe-Mn after 13 d. As the SGO/Fe-Mn was increased to 0.8%, the removal percentage reached 94.0%, i.e., a 23.2% enhancement. Evidently, higher dosage of SGO/Fe-Mn provided more sorption sites for mercury, resulting in less leachability. Upon equilibrium at 72 d, the mercury immobilization efficiencies were 90.3%, 95.0%, 97.9%, and 98.9%, respectively, with the addition of 0.4% SGO/Fe-Mn per the four kinds of leaching tests. When the dosage was increased to 0.8%, the immobilization efficiencies were 96.5%, 97.5%, 98.1%, and 98.9%, respectively. Based on the t -tests, the differences between the equilibrium mercury immobilization efficiencies with 0.4% and 0.8% SGO/Fe-Mn via the H_2O extraction method were statistically significant with a p value of 0.01 at the 0.05 level of significance, whereas the differences via the H_2SO_4 and HNO_3 , CH_3COOH , and CaCl_2 leaching methods were not statistically significant with p values of 0.15, 0.79, and 0.99 (> 0.05), respectively. This phenomena can be explained by the fact

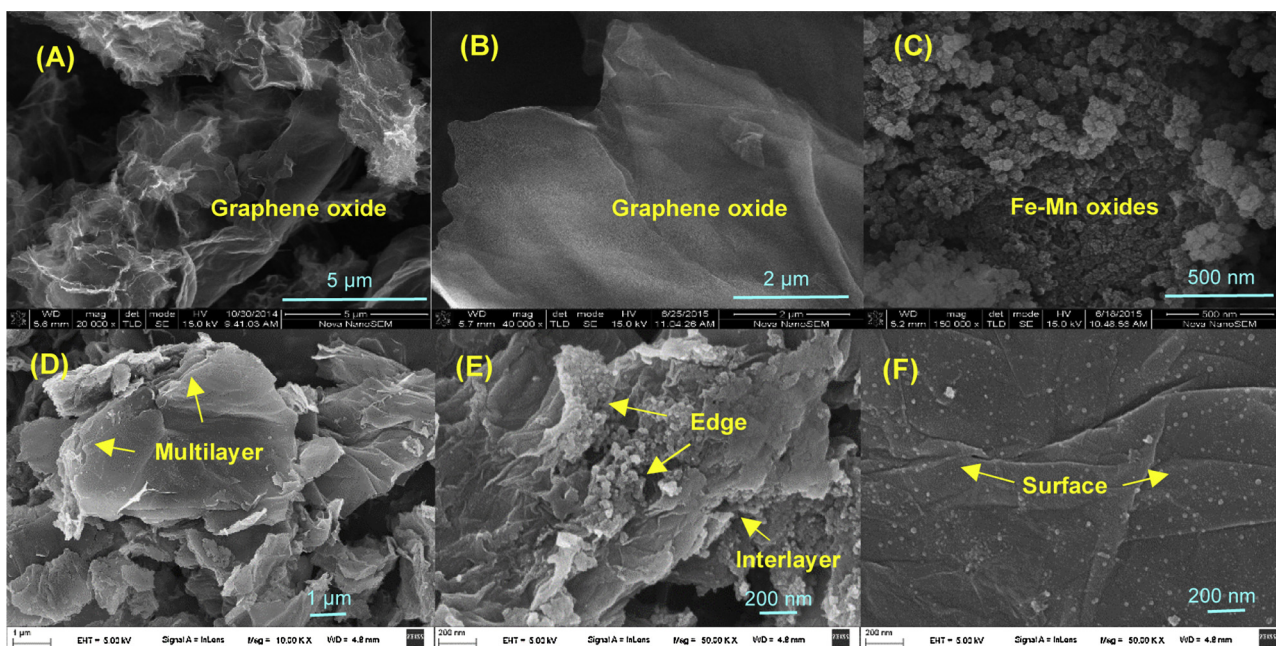


Fig. 1. SEM images of GO (A, B), Fe-Mn oxides (C), and SGO/Fe-Mn (D, E, F).

that mercury was transformed from the more available mercury fractions (EX and CB fractions) to the less available forms (OX, OM, and RS fractions) with the application of SGO/Fe-Mn over time as described in section 3.3.

It should be noted that the H₂SO₄ and HNO₃ method (HJ/T299-2007) has been applied as a standard method for classifying hazardous wastes including mercury. The H₂SO₄ and HNO₃ leachable mercury of the untreated soil (160.0 μg L⁻¹) exceeded the threshold (100.0 μg L⁻¹) of identification standard for hazardous wastes of China (GB 5085.3-2007). When treated with 0.4% and 0.8% of SGO/Fe-Mn, the H₂SO₄ and HNO₃ leachable mercury was reduced by 37.7% (after 3 d) and 42.6% (after 7 d), respectively, i.e., the leachable mercury

concentrations decreased to 99.7 μg L⁻¹ and 91.8 μg L⁻¹, respectively, below the permissible threshold.

A series of batch immobilization tests were carried out at soil moisture contents varying from 0 to 80.0% (i.e., 0%–128.0% of the water holding capacity) to investigate the soil moisture effect on mercury immobilization by 0.4% SGO/Fe-Mn (Fig. 3). As the moisture increased from 0 to 6.0% and further to 12.5%, the mercury immobilization efficiency rose significantly from 75.3% to 95.9% and further to 97.6%. Based on the *t*-tests, the differences between the immobilization efficiencies of mercury at soil moisture contents of 6.0% and 12.5% were statistically significant with a *p* value of 0.03 at the 0.05 level of significance. When the moisture content varied from

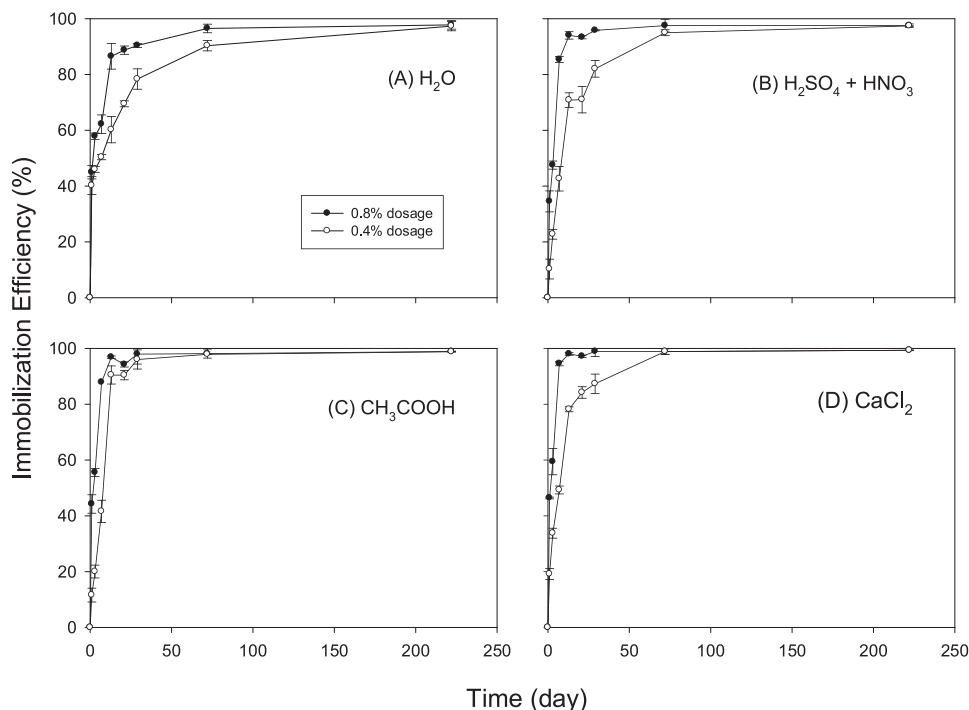


Fig. 2. Effects of remediation time and SGO/Fe-Mn dosage on mercury immobilization.

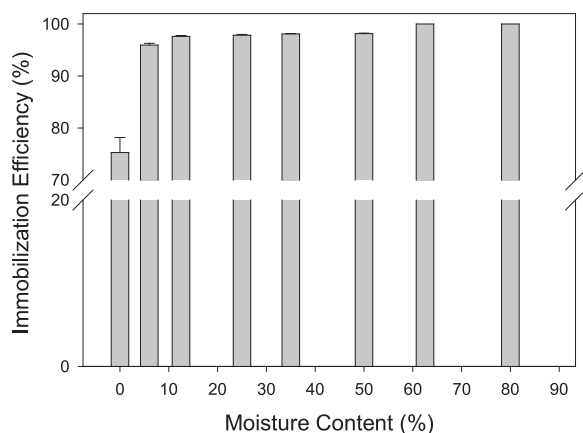


Fig. 3. Effects of soil moisture content on mercury immobilization.

12.5% to 50.0%, the mercury immobilization efficiency remained constant at 97.6–98.1%. Once the soil moisture content reached 62.5% (i.e., 100.0% of water holding capacity), the immobilization efficiency raised to 100.0% ($p < 0.01$). Immobilization of mercury in soil via SGO/Fe-Mn consists of the following steps: (i) desorption of mercury from the contaminated soil into the interstitial water, and (ii) adsorption of desorbed mercury onto SGO/Fe-Mn [25]. Soil moisture can promote the complete mixture between SGO/Fe-Mn and soil and is conducive for mercury to migrate and bind onto SGO/Fe-Mn.

3.3. Mercury immobilization mechanisms by SGO/Fe-Mn

FTIR analysis of SGO/Fe-Mn and Hg-laden soils before and after treatment are shown in Fig. 4. For SGO/Fe-Mn, the peaks at 682, 885, 1025, 1105, 1234, 1405, 1588, 1722, 2181, 2560, 3212, and 3448 cm^{-1} were ascribed to the vibrations of C–S, Si–O, C–O, Si–C, C–O–C, –OH, C=C, C=O, C≡C, –SH, –OH, and –OH/Si–OH groups, respectively [4,17,26]. For Hg-laden soil before treatment, the characteristic peaks at 785, 991, 1440, 1630, and 3620 cm^{-1} were corresponded to C–H, Si–O, –OH, H₂O, and –OH, respectively [4,17,26,27]. Upon SGO/Fe-Mn treatment (0.8% dosage), the FTIR spectra of soil showed similar absorption band to the soil before treatment. Yet, the band of –OH at 1440 and 3620 cm^{-1} increased by 13.6% and 29.4%, respectively, which might be due to the addition of SGO/Fe-Mn, resulting in an increase in the hydroxyl content, promoting the complexation between –OH groups and mercury.

XRD patterns of the soil before and after 0.8% SGO/Fe-Mn

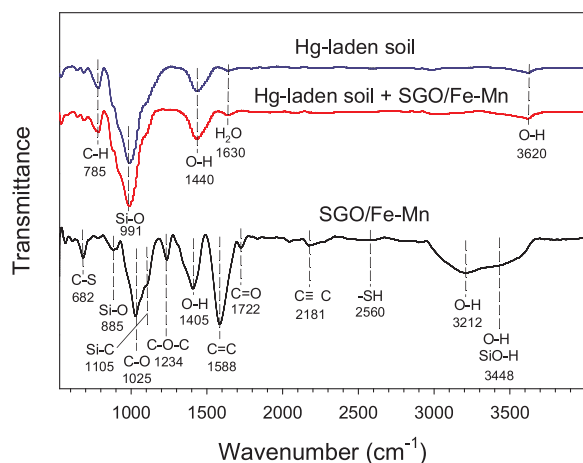


Fig. 4. FTIR analysis of SGO/Fe-Mn and Hg-laden soil before and after treatment.

treatment are compared in Fig. 5. No obvious diffraction peaks are observed for SGO/Fe-Mn (Fig. S1), revealing that SGO/Fe-Mn existed in an amorphous form. The co-existing of Fe oxides and Mn oxides as well as thiol-modification may restrain the formation of crystals [4,17,28]. The main compounds in the Hg-laden soil (Fig. 5A) include silicon oxide (SiO₂, PDF#85-0458), adularia (K₄Al₄Si₁₂O₃₂, PDF#71-0956), calcium aluminum silicate (Ca₃Al₆Si₂O₁₆, PDF#23-0105), lepidocrocite (γ -FeO(OH), PDF#44-1415), goethite (α -FeO(OH), PDF#02-0272), HgO (PDF#05-0596), HgSO₄ (PDF#74-2315), Hg₃(PO₄)₂ (PDF#01-0852), and HgS (PDF#03-0424) (Fig. 5A). Upon SGO/Fe-Mn addition, the peaks at 21.22° ($d = 4.18 \text{ \AA}$), 27.05° ($d = 3.29 \text{ \AA}$), 50.53° ($d = 1.80 \text{ \AA}$), and 28.49° ($d = 3.13 \text{ \AA}$) were enhanced (Fig. 5B), indicating the increase of SiO₂, K₄Al₄Si₁₂O₃₂, Ca₃Al₆Si₂O₁₆, α -FeO(OH), and HgS. Meanwhile, the peak intensities of HgO, HgSO₄, and Hg₃(PO₄)₂ were weakened. These observations might be attributed to surface complexation and chemical precipitation between mercury and SGO/Fe-Mn.

The chemical compositions and oxidation states of SGO/Fe-Mn and the soil before and after 0.8% SGO/Fe-Mn treatment were characterized by XPS (Figs. 6, S2, and S3). For Hg-contaminated soil, the peaks of C1s (Fig. 6A) at 284.6, 286.3, and 289.5 eV were ascribed to C–C/C=C, C–O, and C=O, respectively [4,15,29–31]. The Fe2p peaks (Fig. 6B) at 711.5, 712.3, 714.1, 720.0, and 726.5 eV were characteristic peaks of FeO, Fe₂O₃, FeOOH, Fe³⁺ 2p_{3/2} satellite peak, and Fe2p_{1/2}, respectively [4,15,17,32]. The O1s binding energies (Fig. 6C) at 531.7, 532.5, and 533.3 eV were representative of O²⁻, –OH, and H₂O [33]. The Si2p binding energies (Fig. S3H) around 102.7 and 103.4 eV represented Si–O and C–O–Si–O–M (M=Si or metal), respectively [4,34,35].

Upon SGO/Fe-Mn treatment, for C1s (Fig. 6D), C–C/C=C functional group increased from 38.8% to 47.5%, and C–O group decreased from 47.1% to 38.7%, which was related to surface complexation between SGO/Fe-Mn and mercury [4,36]. For Fe2p (Fig. 6E), the percentage of FeOOH and Fe₂O₃ were increased by 9.6% and 5.1%, respectively, whereas FeO were decreased by 6.9%, indicating the occurrence of the redox reactions. FeOOH and Fe₂O₃ were reported to form the charge distribution multi-site complexation with mercury [4,17,37]. For O1s (Fig. 6F), oxide oxygen (O²⁻) and hydroxyl (–OH) were the main forms of oxygen in the soil. The addition of SGO/Fe-Mn increased the hydroxyl group by 6.2% and reduced the oxide oxygen by 5.8% in soil. Our previous studies revealed that FeOOH and MnOOH were the main metal compounds in SGO/Fe-Mn, providing abundant hydroxyl functional groups, which can promote the surface complexation with mercury [4,15]. The S2p binding energies of SGO/Fe-Mn (Fig. S3D) at 164.3, 163.2, and 168.3 eV were representative of S2p_{1/2} (–SH), S2p_{3/2} (C–S), and oxidized sulfur (e.g., thiosulfate and sulfite), respectively [4,35,38]. The S2p was not observed in the soil before and after treatment (Figs. S3E, F), probably because of the low dosage of SGO/Fe-Mn. Similarly, the Mn2p peaks (Fig. S3A) at 641.1, 642.5, 644.7, 647.5, and 653.9 eV were ascribed to Mn²⁺ for MnO, Mn³⁺ for MnOOH, Mn⁴⁺ for MnO₂, Mn²⁺ 2p_{3/2} satellite peak, and Mn2p_{1/2}, respectively [4,32,39], while no Mn2p was discovered in the soil before and after treatment (Fig. S3B, C). After the SGO/Fe-Mn amendments, Si–O–metal in the soil were slightly increased by 0.9% (Fig. S3H, I), which might be due to the adsorption of mercury onto SiO₂ [40].

The SEP is largely applied to investigate metal distribution among soil fractions, which can offer an indication of metal bioavailability and mobility in soil. The sequential Hg extraction from the soil before and after SGO/Fe-Mn treatment are compared in Fig. 7. For the untreated soil, the mercury species of EX, CB, OX, OM, and RS accounted for 18.5%, 8.9%, 0.5%, 68.2%, and 4.0%, respectively. The application of SGO/Fe-Mn at rates of 0.4% and 0.8% resulted in a substantial shift in mercury speciation from more easily available species (i.e., EX and CB) to much less available species (i.e., OX, OM, and RS) over time. For instance, with the addition of 0.4% SGO/Fe-Mn, the EX and CB fractions decreased from 18.5% and 8.9% for untreated soil to 1.4% and 0.5% after 42 d, and further to 0.4% and 0.2% after 72 d, respectively.

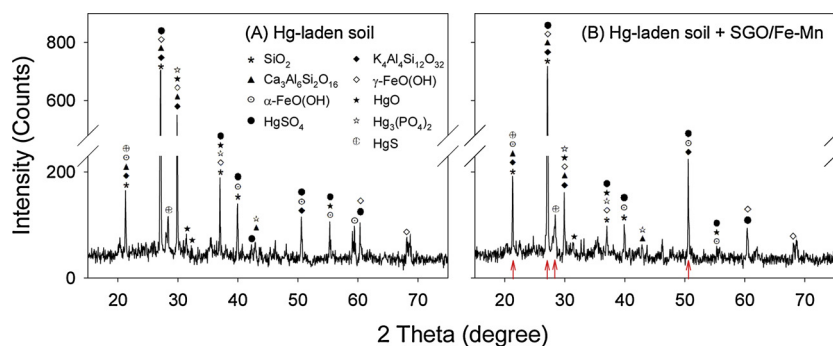


Fig. 5. XRD patterns of Hg-laden soils before (A) and after treatment (B).

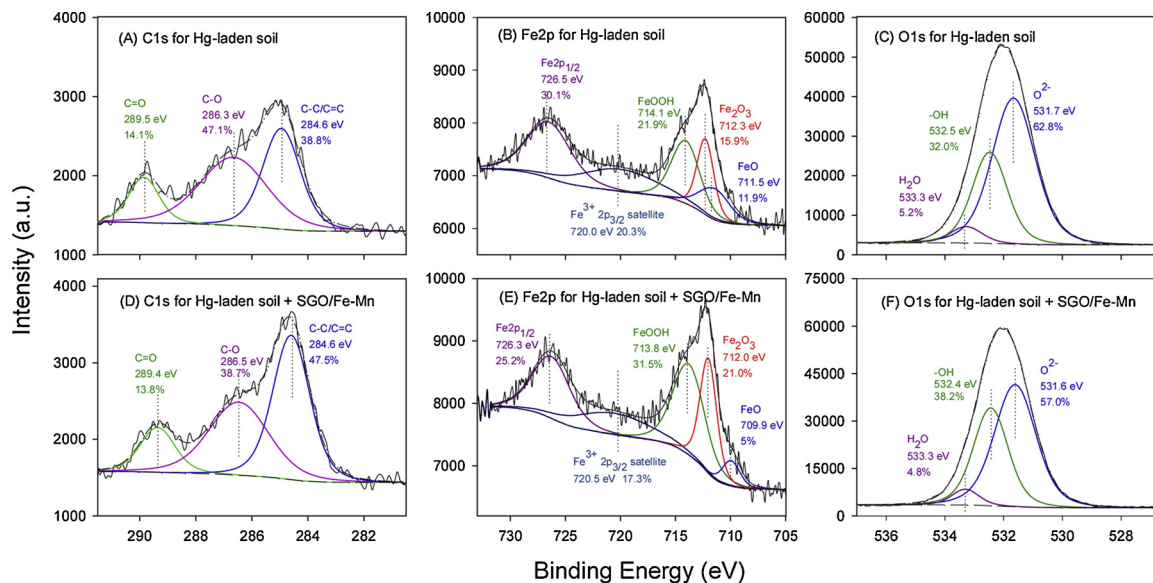


Fig. 6. C1s (A, D), Fe2p (B, E), and O1s (C, F) spectra of Hg-laden soils before and after treatment.

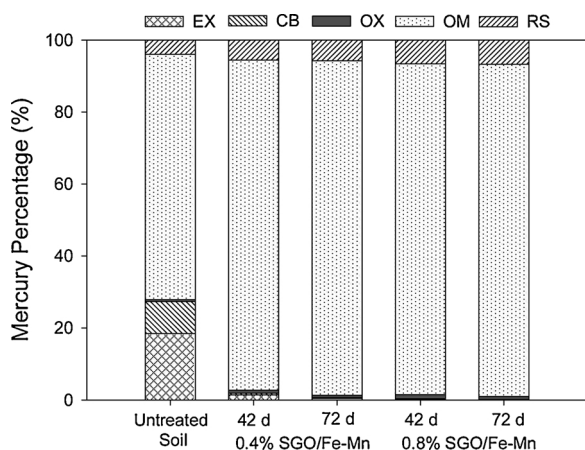


Fig. 7. Effects of treatment time (42 and 72 d) and SGO/Fe-Mn dosage (0.4% and 0.8%) on mercury speciation in soil.

Meanwhile, the OX, OM, and RS fractions increased from 0.5%, 68.2%, and 4.0% for untreated soil to 0.8%, 91.7%, and 5.6% after 42 d, and further to 0.6%, 92.9%, and 5.8% after 72 d, respectively. As the dosage of SGO/Fe-Mn was increased to 0.8%, the EX and CB fractions was decreased whereas OX, OM, and RS fractions was increased. After 42-d treatment, the EX and CB fractions decreased from 1.4% and 0.5% for 0.4% SGO/Fe-Mn to 0.2% and 0.2% for 0.8% SGO/Fe-Mn, respectively. Meanwhile, the OX, OM, and RS fractions increased from 0.8%, 91.7%,

and 5.6% for 0.4% SGO/Fe-Mn to 1.1%, 91.9%, and 6.6% for 0.8% SGO/Fe-Mn, respectively. It should be pointed out that the changes of mercury species after 72 d for the two dosages (0.8% and 0.4%) were not statistically significant (*p* values were 0.11, 0.06, 0.06, 0.38, and 0.67, respectively, based on the *t*-tests for EX, CB, OX, OM, and RS fractions).

SGO/Fe-Mn was rich in -SH, -OH, and O=C-O functional groups, which had strong binding ability to mercury (stability constants were 22.1, 10.6, and 9.7, respectively) [15,31,41–43]. These active sites can immobilize mercury via surface complexation [4,17] and chemical precipitation of HgS, resulting in a conversion of mercury speciation from more easily available species (EX and CB fractions) to less available species (OX, OM, and RS fractions).

3.4. Risk assessment code

The risk levels of mercury in contaminated soil before and after SGO/Fe-Mn treatment are compared (Table S2). The contaminated soil with a RAC value of 27.4% was under medium risk. After 42-d treatment, the RAC value was decreased to 1.9% and 1.7% at SGO/Fe-Mn dosages of 0.4% and 0.8%, respectively, denoting a low risk. As the incubation time continued, after 72 d, the soil was no risk (RAC was 0.7% and 0.6% with the addition of 0.4% and 0.8% SGO/Fe-Mn, respectively). It is clear that the addition of SGO/Fe-Mn reduced the risk of mercury in contaminated soil.

Table 1
Physicochemical properties of Hg-laden soils before and after treatment with SGO/Fe-Mn.

	Hg-laden soil	SGO/Fe-Mn treated soil
pH	8.9	8.3
CEC ^a (mol kg ⁻¹)	0.9	1.2
Available N (mg kg ⁻¹)	24.4	37.8
Available P (mg kg ⁻¹)	4.3	4.2
Available K (mg kg ⁻¹)	121.9	155.9
TOC ^b (mg kg ⁻¹)	6400.0	7200.0
Sand (%)	34.4	–
Silt (%)	51.6	–
Clay (%)	14.0	–

Note: Hg-laden soil was treated with 0.8% (w/w) SGO/Fe-Mn for 72 d.

–: Not detected.

^a CEC: Cation exchange capacity.

^b TOC: Total organic carbon.

3.5. Effect of SGO/Fe-Mn amendment on soil properties

Chemical compositions of the Hg-laden soil were analyzed by XRF. SiO₂ (58.9%), Al₂O₃ (17.2%), CaO (9.1%), Fe₂O₃ (6.9%), K₂O (3.2%), MgO (2.0%), Na₂O (1.0%), and trace amounts of other oxides (the total amount < 1.8%) were detected (Table S3). The Hg content in the soil was determined to be 0.0189% (i.e., 189.0 mg kg⁻¹) according to XRF analysis, which was consistent with our results per US EPA Method 3050B analysis (195.0 mg kg⁻¹).

Selected physicochemical properties of soils are listed in Table 1. The soil texture conformed to the class of silty loam (34.4% sand, 51.6% silt, and 14.0% clay). It was alkaline (soil pH = 8.9) with CEC of 0.9 mol kg⁻¹. The contents of TOC, available N, P, and K were 6400.0, 24.4, 4.3, and 121.9 mg kg⁻¹, respectively. Upon 72-d treatment with 0.8% SGO/Fe-Mn, there was a slight decrease of 0.6 units in soil pH (soil pH = 8.3 after treatment), which can be attributed to the reaction between mercury and thiol and carboxyl functional groups on the surface of SGO/Fe-Mn [4]. It should be noted that the alkaline pH after SGO/Fe-Mn amendment was beneficial to chemical precipitation of mercury [4,17,44]. Soil CEC is associated with the negative charge in soil colloid, affecting the bioavailability of heavy metals [45]. Higher CEC favored stabilization of mercury in soil. The application of SGO/Fe-Mn increased CEC by 0.3 mol kg⁻¹ due to the abundant functional groups (e.g., thiol, carboxyl, and hydroxyl groups) existing on the surface, edge and interlayer [4]. The increase of TOC content from 6400.0 to 7200.0 mg kg⁻¹ indicated that SGO/Fe-Mn introduced carbon source into the soil, which can promote the complexation of metal ions [44]. Furthermore, after SGO/Fe-Mn treatment, the contents of available N and K were increased by 13.4 and 34.0 mg kg⁻¹, respectively, which suggested an improved soil fertility. During the preparation of SGO/Fe-Mn, ammonium hydroxide and KMnO₄ were applied, resulting in retained N and K in the SGO/Fe-Mn. The application of SGO/Fe-Mn exhibited negligible effect on soil available P.

3.6. Long-term stability of SGO/Fe-Mn-immobilized Hg in soil

Long-term effectiveness and performance are important criteria to

Table 2
Immobilization efficiencies and leaching concentrations of mercury in soil after 365-d treatment with SGO/Fe-Mn.

Extraction agent	Soil treated with 0.4% SGO/Fe-Mn		Soil treated with 0.8% SGO/Fe-Mn	
	Immobilization efficiency (%)	Leachable mercury concentration (μg L ⁻¹)	Immobilization efficiency (%)	Leachable mercury concentration (μg L ⁻¹)
H ₂ O	99.3	1.0	99.4	0.9
H ₂ SO ₄ + HNO ₃	99.5	0.8	99.6	0.7
CH ₃ COOH	99.7	0.3	99.7	0.3
CaCl ₂	99.9	0.2	99.9	0.2

evaluate heavy metals remediation technologies. The effect of SGO/Fe-Mn on the immobilization of mercury was examined by monitoring the levels of H₂O, H₂SO₄ and HNO₃, CH₃COOH, and CaCl₂ extractable mercury over one year. Following the application of SGO/Fe-Mn at dosages of 0.4% and 0.8%, the Hg concentration in four leaching solutions were reduced by 99.4%–99.9% (0.8% SGO/Fe-Mn) and 99.3%–99.9% (0.4% SGO/Fe-Mn) after one year (Table 2), compared to 96.5%–98.9% (0.8% SGO/Fe-Mn) and 90.3%–98.9% (0.4% SGO/Fe-Mn) upon equilibrium after 72 d. Correspondingly, the leaching concentrations of mercury decreased from 2.0–5.3 μg L⁻¹ (0.8% SGO/Fe-Mn) and 2.3–14.5 μg L⁻¹ (0.4% SGO/Fe-Mn) after 72-d treatment to 0.2–0.9 μg L⁻¹ (0.8% SGO/Fe-Mn) and 0.2–1.0 μg L⁻¹ (0.4% SGO/Fe-Mn) after 365-d treatment. Clearly, over one year, the H₂SO₄ and HNO₃ leachable mercury concentration met the third-level quality standard of 1.0 μg L⁻¹ for mercury in groundwater (GB/T 14848-2017, China). The observations proved that SGO/Fe-Mn can facilitate long-term immobilization of mercury in soil.

4. Conclusions

This work investigated the immobilization effectiveness and mechanisms of SGO/Fe-Mn for *in situ* remediation of mercury-contaminated soil. The immobilization was tested using various leaching conditions, namely, H₂O, H₂SO₄ and HNO₃, CH₃COOH, and CaCl₂ solutions to simulate surface water or groundwater, acidic rain, landfill leachate, and bioavailable mercury, respectively. SGO/Fe-Mn at dosages of 0.4% and 0.8% effectively immobilized mercury in the soil, the leachability were significantly reduced by 90.3–98.9% and 96.5–98.9%, respectively, upon equilibrium within 72 d. Increasing the soil moisture content from 0% to 12.5% significantly enhanced the immobilization efficiency from 75.0% to 97.6%. Further increasing the moisture content to 62.5% improved the immobilization efficiency to 100.0%. SEP revealed that the more available mercury fractions (EX and CB) were transformed to the less available forms (OX, OM, and RS) with the application of SGO/Fe-Mn, and the environmental risk of Hg in the soil was greatly reduced. Surface complexation and chemical precipitation were dominant immobilization mechanisms. The addition of SGO/Fe-Mn also increased soil cation exchange capacity, available N and K, and total organic carbon, and can be used as an effective way of improving soil properties besides remediating Hg-contaminated soil. The immobilized mercury remained stable over one year. This study provides compelling evidence that SGO/Fe-Mn are promising for *in situ* immobilization of mercury in soil.

Acknowledgements

The authors gratefully acknowledge the partial financial supports from National Natural Science Foundation of China (41503085, 41807115), the Guangzhou Science and Technology Program key projects (No. 201804020050), the Fundamental Research Funds for the Central Universities, and the Guangdong Innovative and Entrepreneurial Research Team Program (No.2016ZT06N569).

Appendix A. Supplementary data

Supplementary material related to this article can be found, in the online version, at doi:<https://doi.org/10.1016/j.jhazmat.2019.03.132>.

References

- [1] J. Wang, X. Feng, C.W. Anderson, Y. Xing, L. Shang, Remediation of mercury contaminated sites – a review, *J. Hazard. Mater.* 221–222 (2012) 1–18.
- [2] J. Mutter, J. Naumann, C. Sadaghiani, H. Walach, G. Drasch, Amalgam studies: disregarding basic principles of mercury toxicity, *Int. J. Hyg. Environ. Heal.* 207 (2004) 391–397.
- [3] P. Holmes, K.A. James, L.S. Levy, Is low-level environmental mercury exposure of concern to human health? *Sci. Total Environ.* 408 (2009) 171–182.
- [4] Y. Huang, J. Tang, L. Gai, Y. Gong, H. Guan, R. He, H. Lyu, Different approaches for preparing a novel thiol-functionalized graphene oxide/Fe-Mn and its application for aqueous methylmercury removal, *Chem. Eng. J.* 319 (2017) 229–239.
- [5] J.D. Subirés-Muñoz, A. García-Rubio, C. Vereda-Alonso, C. Gómez-Lahoz, J.M. Rodríguez-Maroto, F. García-Herruzo, J.M. Paz-García, Feasibility study of the use of different extractant agents in the remediation of a mercury contaminated soil from Almadén, Sep. Purif. Technol. 79 (2011) 151–156.
- [6] A. Navarro, I. Cañadas, D. Martínez, J. Rodríguez, J.L. Mendoza, Application of solar thermal desorption to remediation of mercury-contaminated soils, *Sol. Energy* 83 (2009) 1405–1414.
- [7] F. Ma, C. Peng, D. Hou, B. Wu, Q. Zhang, F. Li, Q. Gu, Citric acid facilitated thermal treatment: an innovative method for the remediation of mercury contaminated soil, *J. Hazard. Mater.* 300 (2015) 546–552.
- [8] F. Ma, Q. Zhang, D. Xu, D. Hou, F. Li, Q. Gu, Mercury removal from contaminated soil by thermal treatment with FeCl₃ at reduced temperature, *Chemosphere* 117 (2014) 388–393.
- [9] A. García-Rubio, J.M. Rodríguez-Maroto, C. Gómez-Lahoz, F. García-Herruzo, C. Vereda-Alonso, Electrokinetic remediation: the use of mercury speciation for feasibility studies applied to a contaminated soil from Almadén, *Electrochim. Acta* 56 (2011) 9303–9310.
- [10] B. Smolinska, Green waste compost as an amendment during induced phytoextraction of mercury-contaminated soil, *Environ. Sci. Pollut. Res.* 22 (2015) 3528–3537.
- [11] F. He, W. Wang, J.W. Moon, J. Howe, E.M. Pierce, L. Liang, Rapid removal of Hg(II) from aqueous solutions using thiol-functionalized Zn-doped biomagnetite particles, *ACS Appl. Mater. Interfaces* 4 (2012) 4373–4379.
- [12] Y. Niu, R. Qu, X. Liu, L. Mu, B. Bu, Y. Sun, H. Chen, Y. Meng, L. Meng, L. Cheng, Thiol-functionalized polysilsesquioxane as efficient adsorbent for adsorption of Hg (II) and Mn(II) from aqueous solution, *Mater. Res. Bull.* 52 (2014) 134–142.
- [13] X.Y. Zhang, Q.C. Wang, S.Q. Zhang, X.J. Sun, Z.S. Zhang, Stabilization/solidification (S/S) of mercury-contaminated hazardous wastes using thiol-functionalized zeolite and Portland cement, *J. Hazard. Mater.* 168 (2009) 1575–1580.
- [14] D. O'Connor, T. Peng, G. Li, S. Wang, L. Duan, J. Mulder, G. Cornelissen, Z. Cheng, S. Yang, D. Hou, Sulfur-modified rice husk biochar: a green method for the remediation of mercury contaminated soil, *Sci. Total Environ.* 621 (2018) 819–826.
- [15] Y. Huang, Y. Gong, J. Tang, S. Xia, Effective removal of inorganic mercury and methylmercury from aqueous solution using novel thiol-functionalized graphene oxide/Fe-Mn composite, *J. Hazard. Mater.* 366 (2019) 130–139.
- [16] Y. Gong, Y. Liu, Z. Xiong, D. Kaback, D. Zhao, Immobilization of mercury in field soil and sediment using carboxymethyl cellulose stabilized iron sulfide nanoparticles, *Nanotechnology* 23 (2012) 294007.
- [17] J. Tang, Y. Huang, Y. Gong, H. Lyu, Q. Wang, J. Ma, Preparation of a novel graphene oxide/Fe-Mn composite and its application for aqueous Hg(II) removal, *J. Hazard. Mater.* 316 (2016) 151–158.
- [18] X. Cao, L. Ma, Y. Liang, B. Gao, W. Harris, Simultaneous immobilization of lead and atrazine in contaminated soils using dairy-manure biochar, *Environ. Sci. Technol.* 45 (2011) 4884–4889.
- [19] H. Su, Z. Fang, P.E. Tsang, L. Zheng, W. Cheng, J. Fang, D. Zhao, Remediation of hexavalent chromium contaminated soil by biochar-supported zero-valent iron nanoparticles, *J. Hazard. Mater.* 318 (2016) 533–540.
- [20] A. Tessier, P.G.C. Campbell, M. Bisson, Sequential extraction procedure for the speciation of particulate trace metals, *Anal. Chem.* 51 (1979) 844–851.
- [21] X. Xu, X. Hu, Z. Ding, Y. Chen, Effects of coprolysis of sludge with calcium carbonate and calcium hydrogen phosphate on chemical stability of carbon and release of toxic elements in the resultant biochars, *Chemosphere* 189 (2017) 76–85.
- [22] X. Liu, Y. Wang, C. Gui, P. Li, J. Zhang, H. Zhong, Y. Wei, Chemical forms and risk assessment of heavy metals in sludge-biochar produced by microwave-induced low temperature pyrolysis, *RSC Adv.* 6 (2016) 101960–101967.
- [23] G. Liu, S. Ling, X. Zhan, Z. Lin, W. Zhang, K. Lin, Interaction effects and mechanism of Pb pollution and soil microorganism in the presence of earthworm, *Chemosphere* 173 (2017) 227–234.
- [24] G. Perin, L. Craboledda, M. Luchese, R. Cirillo, L. Dotta, M.L. Zanette, A.A. Orio, Heavy metal speciation in the sediments of northern Adriatic Sea. A new approach for environmental toxicity determination, *Heavy Met. Environ.* 2 (1985) 454–456.
- [25] T. Suzuki, S. Kakoyama, T. Nomura, C. Fukuoka, M. Niinae, Lead(II) immobilization in kaolinite at near-neutral pH conditions using titanium-based compounds, *J. Environ. Chem. Eng.* 5 (2017) 3129–3135.
- [26] H. Lyu, J. Tang, Y. Huang, L. Gai, E.Y. Zeng, K. Liber, Y. Gong, Removal of hexavalent chromium from aqueous solutions by a novel biochar supported nanoscale iron sulfide composite, *Chem. Eng. J.* 322 (2017) 516–524.
- [27] S. Xia, Y. Huang, J. Tang, L. Wang, Preparation of various thiol-functionalized carbon-based materials for enhanced removal of mercury from aqueous solution, *Environ. Sci. Pollut. Res.* (2019), 1–12.
- [28] G. Zhang, J. Qu, H. Liu, R. Liu, R. Wu, Preparation and evaluation of a novel Fe-Mn binary oxide adsorbent for effective arsenite removal, *Water Res.* 41 (2007) 1921–1928.
- [29] H. Fu, D. Zhu, Graphene oxide-facilitated reduction of nitrobenzene in sulfide-containing aqueous solutions, *Environ. Sci. Technol.* 47 (2013) 4204–4210.
- [30] T. Herranz, S. Rojas, M. Ojeda, F.J. Perez-Alonso, P. Terreros, K. Pirota, J.L.G. Fierro, Synthesis, structural features, and reactivity of Fe-Mn mixed oxides prepared by microemulsion, *Chem. Mater.* 18 (2006) 2364–2375.
- [31] Y. Huang, S. Xia, J. Lyu, J. Tang, Highly efficient removal of aqueous Hg²⁺ and CH₃Hg⁺ by selective modification of biochar with 3-mercaptopropyltrimethoxysilane, *Chem. Eng. J.* 360 (2019) 1646–1655.
- [32] M.C. Biesinger, B.P. Payne, A.P. Grosvenor, L.W.M. Lau, A.R. Gerson, R.S.C. Smart, Resolving surface chemical states in XPS analysis of first row transition metals, oxides and hydroxides: Cr, Mn, Fe, Co and Ni, *Appl. Surf. Sci.* 257 (2011) 2717–2730.
- [33] Y. Zhang, M. Yang, X.-M. Dou, H. He, D.-S. Wang, Arsenate adsorption on an Fe-Ce bimetal oxide adsorbent: role of surface properties, *Environ. Sci. Technol.* 39 (2005) 7246–7253.
- [34] B. Carriere, J.P. Deville, D. Brion, J. Escard, X-ray photoelectron study of some silicon-oxygen compounds, *J. Electron. Spectrosc. Relat. Phenom.* 10 (1977) 85–91.
- [35] C.D. Wagner, W.M. Riggs, L.E. Davis, J.F. Moulder, G.E. Muilenberg, Handbook of X-Ray Photoelectron Spectroscopy, Perkin-Elmer Corporation Physical Electronics Division, 1979.
- [36] C.J. Daughney, S.D. Siciliano, A.N. Rencz, D. Lean, D. Fortin, Hg(II) adsorption by bacteria: a surface complexation model and its application to shallow acidic lakes and wetlands in Kejimikujik National Park, Nova Scotia, Canada, *Environ. Sci. Technol.* 36 (2002) 1546–1553.
- [37] J.E. Mangold, C.M. Park, H.M. Liljestrand, L.E. Katz, Surface complexation modeling of Hg(II) adsorption at the goethite/water interface using the charge distribution multi-site complexation (CD-MUSIC) model, *J. Colloid Interface Sci.* 418 (2014) 147–161.
- [38] S.-A. Wohlgemuth, F. Vilela, M.-M. Titirici, M. Antonietti, A one-pot hydrothermal synthesis of tunable dual heteroatom-doped carbon microspheres, *Green. Chem.* 14 (2012) 741.
- [39] J. Li, J. Chen, Y. Yu, C. He, Fe-Mn-Ce/ceramic powder composite catalyst for highly volatile elemental mercury removal in simulated coal-fired flue gas, *J. Ind. Eng. Chem.* 25 (2015) 352–358.
- [40] C. Tiffreau, J. Lützenkirchen, P. Behra, Modeling the adsorption of mercury(II) on (hydr)oxides: i. Amorphous iron oxide and α-quartz, *J. Colloid Interface Sci.* 172 (1995) 82–93.
- [41] S.-J. Yoon, L.M. Diener, P.R. Bloom, E.A. Nater, W.F. Bleam, X-ray absorption studies of CH₃Hg⁺-binding sites in humic substances, *Geochim. Cosmochim. Acta* 69 (2005) 1111–1121.
- [42] U. Skyllberg, J. Qian, W. Frech, K. Xia, W.F. Bleam, Distribution of mercury, methyl mercury and organic sulphur species in soil, soil solution and stream of a boreal forest catchment, *Biogeochemistry* 64 (2003) 53–76.
- [43] E. Tipping, Modelling the interactions of Hg(II) and methylmercury with humic substances using WHAM/Model VI, *Appl. Geochem.* 22 (2007) 1624–1635.
- [44] F. Guo, C. Ding, Z. Zhou, G. Huang, X. Wang, Stability of immobilization remediation of several amendments on cadmium contaminated soils as affected by simulated soil acidification, *Ecotoxicol. Environ. Saf.* 161 (2018) 164–172.
- [45] X. Zhai, Z. Li, B. Huang, N. Luo, M. Huang, Q. Zhang, G. Zeng, Remediation of multiple heavy metal-contaminated soil through the combination of soil washing and in situ immobilization, *Sci. Total Environ.* 635 (2018) 92–99.